Advanced Powder Technology xxx (2017) xxx–xxx

Contents lists available at ScienceDirect

Advanced Powder Technology

journal homepage: www.elsevier.com/locate/apt

Original Research Paper

Fabrication and anisotropic electronic property for oriented $Li_{1+x-y}Nb_{1-x-3y}Ti_{x+4y}O_3$ solid solution by slip casting in a high magnetic field

Hiromi Nakano [a,*], Shohei Furuya [a], Motohiro Yuasa [b], Tohru S. Suzuki [c], Hitoshi Ohsato [d]

[a] Toyohashi University of Technology, 1-1 Hibariga-oka, Tempaku, Toyohashi 441-8580, Japan
[b] Doshisya University, 1-3 Miyakodani, Tatara, Kyotanabe 610-0394, Japan
[c] National Institute for Materials Science, 1-2-1 Sengen, Tsukuba 305-0047, Japan
[d] Nagoya Industrial Science Research Institute, 1-13 Yotsuya-dori, Chikusa-ku, Nagoya 464-0819, Japan

ARTICLE INFO

Article history:
Received 18 May 2017
Received in revised form 9 June 2017
Accepted 20 June 2017
Available online xxxx

Keywords:
Li-Nb-Ti-O solid solution
Grain orientation
Superstructure
Crystal structure
Anisotropic electric property

ABSTRACT

The $Li_{1+x-y}Nb_{1-x-3y}Ti_{x+4y}O_3$ ($0.06 \le x \le 0.33$, $0 \le y \le 0.09$) (hereafter LNT), forms a unique and periodical structure in the Li_2O-Nb_2O_5-TiO_2 ternary system. In this work, toward application of the unique qualities of an electro-ceramic, we fabricated oriented LNT balk ceramics by slip casting in a strong magnetic field of 12 T using various sizes of particles. The *c*-axis of the LNT powders was aligned parallel to the magnetic field. As a result, we found anisotropic- and unique- electric properties which were caused by a superstructure with intergrowth layers of corundum-type $[Ti_2O_3]^{2+}$. The *Qf* value parallel to the *c*-axis was about five times greater than that of perpendicular to the *c*-axis. We first clarified the mechanism showing that the anisotropic *Qf* value was caused by the anisotropic electron conductivity and the anisotropic bonding strength in the superstructure.

1. Introduction

In the Li_2O-Nb_2O_5-TiO_2 system, $Li_{1+x-y}Nb_{1-x-3y}Ti_{x+4y}O_3$ ($0.06 \le x \le 0.33$, $0 \le y \le 0.09$) (LNT) forms with a superstructure, and this is referred to as the M-phase. The superstructure of the M-phase is formed by periodical insertion of an intergrowth layer of corundum-type $[Ti_2O_3]^{2+}$ in a matrix having a trigonal structure. Since the discovery of the M-phase by Castrejon et al. [1,2], related structures have been investigated [3–6]. The relationship between its dielectric property and the period of the intergrowth layer of the M-phase has also been studied [7,8]. To enable the application of this unique structure as a host material of phosphor, new phosphors were investigated based on LNT or related compounds fabricated by conventional solid state reaction [9–11].

The controlled development of texture has recently become a topic of interest in ceramic processing, since it allows for improved tailoring of the materials' properties. The anisotropy structure of an M-phase solid solution was synthesized, in which rod-precipitates were arranged regularly by a crystal growth method [12]. An oriented thin film of $Li_{1.18}Nb_{0.82}Ti_{0.18}O_3$ on the Al_2O_3 (0001) substrate was prepared by a sol-gel and spin-coating process, however the orientation degree of the thin film was reported to be low [13]. A strong magnetic field has been used to control the development of texture, even in feeble magnetic ceramics such as Al_2O_3, ZnO, AlN, SiC, and TiO_2 [14–18].

In this paper, we fabricated oriented LNT bulk ceramics by slip casting in a strong magnetic field of 12 T and clarified the relationship between the unique qualities and the crystal structure. We will discuss here the important mechanism analyzed for appearance of the anisotropic and its unique properties.

2. Experimental procedure

2.1. Fabrication of materials

The starting materials used were Li_2CO_3, Nb_2O_5 and TiO_2 (>99.99% grade) to prepare solid solutions of LNT. The four compositions, in which $Li_{1.03}Nb_{0.97}Ti_{0.03}O_3$, $Li_{1.11}Nb_{0.89}Ti_{0.11}O_3$, $Li_{1.25}Nb_{0.75}Ti_{0.25}O_3$, $Li_{1.14}Nb_{0.78}Ti_{0.24}O_3$, followed the general formula $Li_{1+x-y}Nb_{1-x-3y}Ti_{x+4y}O_3$. The Ti content (mol%) of the specimens are 3%, 10% and 20%, as shown in Fig. 1. The LNT powders were mixed and calcined at 1273 K for 5 h and continuously at 1393 K for 24 h by an electric furnace in air. The sintering at 1373 K was

* Corresponding author.
E-mail address: hiromi@crfc.tut.ac.jp (H. Nakano).

http://dx.doi.org/10.1016/j.apt.2017.06.020

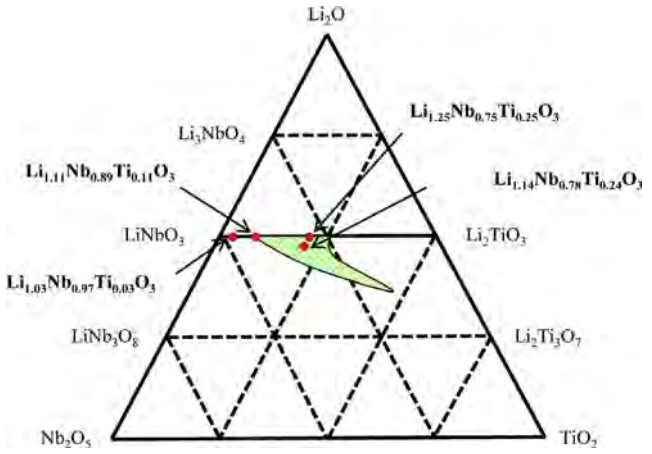

Fig. 1. LNT compositions in ternary phase system.

repeated until the X-ray diffraction (XRD) patterns of resultant powders were free of impurity peaks. The LNT ceramic powders were pulverized to be various grain sizes by planetary ball-milling (P-6, Fritsch Japan Co., Ltd.) and then used to prepare slurries. The particle distribution was measured by using particle sizer (Analysette 22, Fritsch Japan Co., Ltd.). Aqueous slurries containing 15.0 vol% solids were prepared with added polyelectrolyte (poly ammonium acrylate A-6114, Toaghosei, Co., Japan) to ensure dispersion. A strong magnetic field of 12 T was applied to the slurries during slip casting. The direction of the magnetic field was parallel or perpendicular to the casting direction. The specimen was formed with the diameter of 11 mm and the height (d) of about 22 mm (h) by a slip casting process because the measurement of the electrical properties is needed to d/h = 1.8–2.3. The green compact was densified by cold isostatic pressing at 392 MPa and then sintered at 1373 K for 15 h.

2.2. Characterization and simulation

Structure analysis was carried out by X-ray diffraction (XRD) using a RINT 2500 (Rigaku Co., Ltd. Japan) operating at 40 kV and 200 mA. Microstructure images were observed by scanning electron microscope (SEM) using an SU8000 (Hitachi, Tokyo, Japan) operating at 3 kV. High-resolution transmission electron microscope TEM images and selected area electron diffraction (SAED) patterns were observed by 2100 F (JEOL, Tokyo, Japan) operating at 200 kV equipped with energy-dispersed spectroscopy (EDS).

The ratio of Ti^{4+}/Ti^{3+} was measured by X-ray absorption fine structure spectroscopy (XAFS) at beam line BL5S1 in the Aichi Synchrotron Center with fluorescence mode at room temperature. The simulation of the XAFS was undertaken using Artemis software [19].

The microwave dielectric properties were measured using a pair of parallel conducting Cu plates in the TE011 Mode, using Hakki and Coleman's method (JIS R 1627-1996).

First-principles calculations were carried out using the Cambridge Serial Total Energy Package (CASTEP) [20], in which density functional theory [21,22] was used with a plane wave basis set. The plane-wave energy cutoff was set to 400 eV with a Gaussian smearing of 0.1 eV. The exchange-correlation interactions were treated using the spin-polarized version of the generalized gradient approximation within the scheme of Perdew-Burke-Ernzerhof [23]. The ultrasoft pseudopotentials [24] represented in reciprocal space were used for all elements. The Brillouin zone was sampled using a Monkhorst-Pack $5 \times 5 \times 2$, and $5 \times 2 \times 1$ k-point mesh according to the cell size. In the structural optimization, all atomic positions were fully relaxed until the Hellmann-Feynman force on each atom was reduced to within 0.01 eV/Å.

3. Results

3.1. Effect of particle sizes on the orientation for slip casting

In order to fabricate high oriented LNT bulk ceramics by slip casting in a magnetic field, the effect of particle sizes on the orientation was investigated. The particle sizes, dispersibility and sedimentation velocity are the important factors for the slip casting method. The $Li_{1.03}Nb_{0.97}Ti_{0.03}O_3$ ceramic powders were pulverized into small particles by ball-milling, which was repeated several times. Fig. 2 shows XRD patterns of top-plane in oriented $Li_{1.03}Nb_{0.97}Ti_{0.03}O_3$ ceramics by slip casting using crushed powders with several grain sizes. The top-plane is the perpendicular to the magnetic direction, as indicated by picture. The $Li_{1.03}Nb_{0.97}Ti_{0.03}O_3$ ceramic has a basic $LiNbO_3$ type structure without a superstructure. Consequently, single peaks of (006) and (00$\underline{12}$) were detected with very small intensities in the random specimen. On the other hand, strong peaks of (00l) were observed in the top-plane of the oriented specimens. As a result, the c-axis of the LNT powders was aligned parallel to the magnetic field. The samples prepared from the powders of 3.56 and 0.46 μm showed low orientation degrees. The sample prepared from the powder of 2.65 μm showed the highest orientation degree in the various grain sizes.

3.2. Fabrication and characterization of oriented LNT ceramics

3.2.1. Magnetic direction parallel to the casting direction

The oriented LNT ceramics were fabricated with various compositions of $Li_{1.03}Nb_{0.97}Ti_{0.03}O_3$, $Li_{1.11}Nb_{0.89}Ti_{0.11}O_3$, $Li_{1.25}Nb_{0.75}Ti_{0.25}O_3$ and $Li_{1.14}Nb_{0.78}Ti_{0.24}O_3$ using slurries including the particles with a size of 2–3 μm and the direction of the magnetic field was parallel to the casting direction. Fig. 3 shows XRD patterns of top-plane in the oriented LNT ceramics. The c-axis of the LNT with various compositions was also aligned parallel to the magnetic field. The peak shifted to a high angle with increasing Ti content, because the lattice constant of the c-axis became shorter with increasing Ti content [25]. Interestingly, the satellite peaks were detected around the peaks of (006) and (00$\underline{12}$) in the oriented specimens, although these satellite peaks around (00l) have never been observed in the random specimens (in Fig. 2). The spacing of the satellite reflections became wider with increasing the Ti content, as indicated by the arrows. The periodical structures of the LNT ceramics can be seen in the TEM images. Fig. 4 shows TEM images and SAED patterns of oriented LNT ceramics taken from [010] axis. TEM data showed that the period was formed by insertion of the intergrowth layers by the doping of Ti ions. The periods of the intergrowth layers are 14.3 nm in $Li_{1.11}Nb_{0.89}Ti_{0.11}O_3$ and 5.8 nm in $Li_{1.11}Nb_{0.89}Ti_{0.11}O_3$. The period became narrower with increasing Ti content. Accordingly, the period of the satellite peaks in the XRD patterns became wider in the reciprocal lattice with increasing Ti content. The period of $Li_{1.25}Nb_{0.75}Ti_{0.25}O_3$ and $Li_{1.14}Nb_{0.78}Ti_{0.24}O_3$ were almost the same because Ti content is 20 mol% (Fig. 1) [25].

The orientation degrees of each grain can be calculated from the tilting data in the SAED patterns as following equation [26].

$$\varphi = \cos^{-1}(\cos x \cdot \cos y) \tag{1}$$

$$\theta = \tan^{-1}(\tan y / \sin x) \tag{2}$$

Here, x and y are measured angle x-axis and y-axis, respectively in the TEM device. φ is the degree of tilting angle from the basis [001] axis. θ is the direction of tilting on the two-dimensional plane.

Please cite this article in press as: H. Nakano et al., Fabrication and anisotropic electronic property for oriented $Li_{1+x-y}Nb_{1-x-3y}Ti_{x+4y}O_3$ solid solution by slip casting in a high magnetic field, Advanced Powder Technology (2017), http://dx.doi.org/10.1016/j.apt.2017.06.020

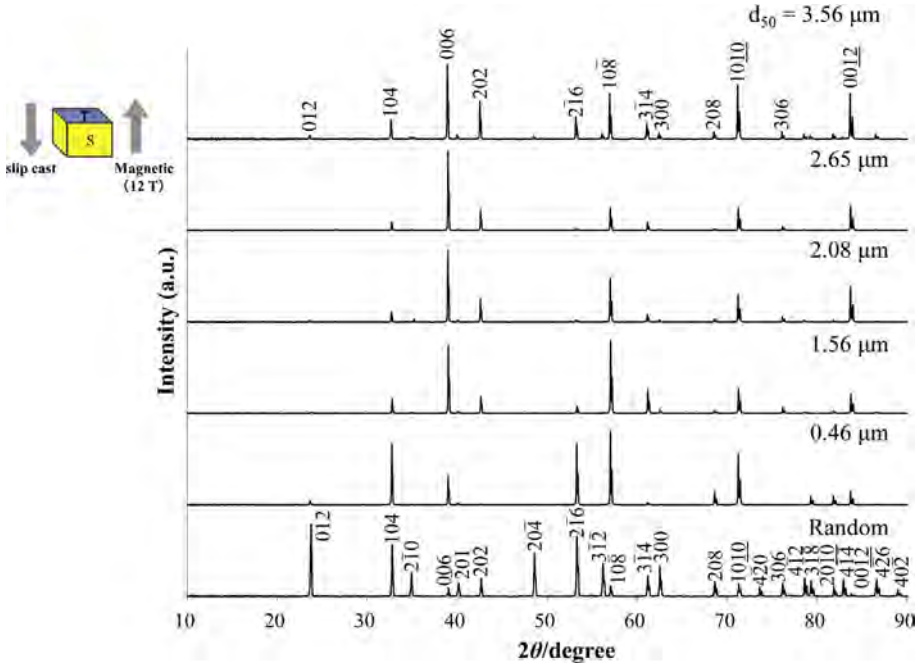

Fig. 2. XRD patterns of top-plane in oriented $Li_{1.03}Nb_{0.97}Ti_{0.03}O_3$ by slip casting using crushed powders with several grain sizes.

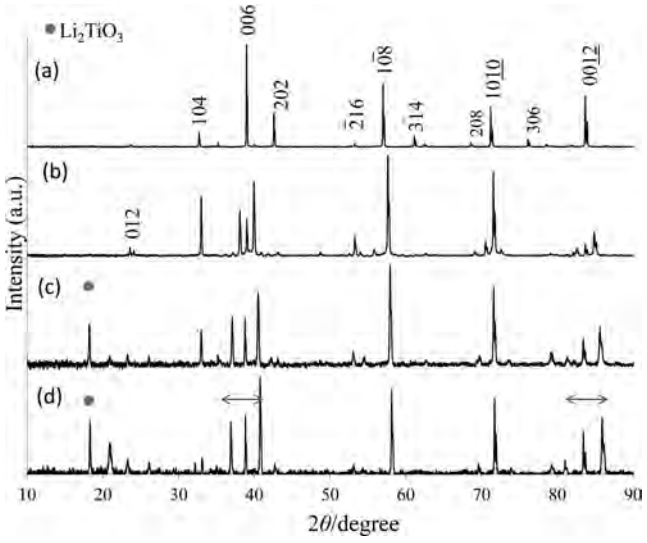

Fig. 3. XRD patterns of top-plane in oriented LNT ceramics, (a) $Li_{1.03}Nb_{0.97}Ti_{0.03}O_3$, (b) $Li_{1.11}Nb_{0.89}Ti_{0.11}O_3$, (c) $Li_{1.25}Nb_{0.75}Ti_{0.25}O_3$ and (d) $Li_{1.14}Nb_{0.78}Ti_{0.24}O_3$.

Fig. 5 shows the TEM images and SAED pattern of $Li_{1.11}Nb_{0.89}Ti_{0.11}O_3$ in (a) and the calculated tilting angles in (b). The results showed that the tilting angles in the observed grains were approximately within 11°.

3.2.2. Magnetic direction perpendicular to the casting direction

In order to undertake measurement of the electrical property, another oriented specimen was made, in which the direction of the magnetic field was perpendicular to the casting direction. Fig. 6 shows XRD patterns of $Li_{1.25}Nb_{0.75}Ti_{0.25}O_3$ ceramics on top-plane in magnetic parallel to the casting direction and side-plane in the specimen perpendicular to the casting direction. The bottom data is a random specimen without a magnetic field. The orientation degrees were almost the same between the two magnetic directions. The *c*-axis of the LNT with various compositions was also aligned parallel to the magnetic field.

3.3. Electric properties of oriented LNT ceramics

3.3.1. Electric resistivity

We measured the electric resistivity of the oriented specimens with a composition of $Li_{1.11}Nb_{0.89}Ti_{0.11}O_3$ and $Li_{1.25}Nb_{0.75}Ti_{0.25}O_3$ in the electric fields of 0 to 30 V and compared the two measure-

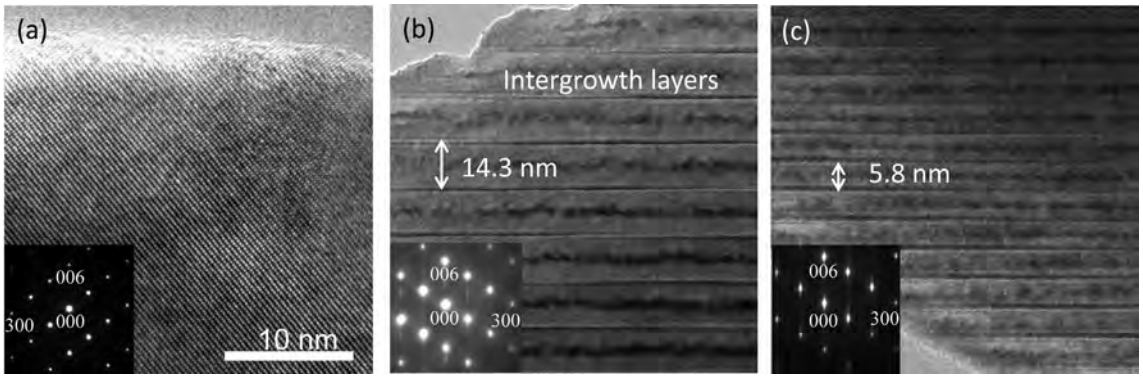

Fig. 4. TEM images and SAED patterns of oriented LNT ceramics taken from [010] axis, (a) $Li_{1.03}Nb_{0.97}Ti_{0.03}O_3$, (b) $Li_{1.11}Nb_{0.89}Ti_{0.11}O_3$ and (c) $Li_{1.25}Nb_{0.75}Ti_{0.25}O_3$.

Please cite this article in press as: H. Nakano et al., Fabrication and anisotropic electronic property for oriented $Li_{1+x-y}Nb_{1-x-3y}Ti_{x+4y}O_3$ solid solution by slip casting in a high magnetic field, Advanced Powder Technology (2017), http://dx.doi.org/10.1016/j.apt.2017.06.020

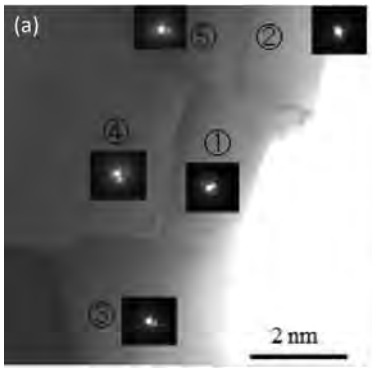

(b) grain	Φ degrees
①	11.0
②	6.5
③	4.0
④	1.6
⑤	3.2

Fig. 5. TEM images and SAED patterns of $Li_{1.11}Nb_{0.89}Ti_{0.11}O_3$ in (a) and calculated tilting angles in (b).

ment directions; perpendicular to the *c*-axis and parallel to the *c*-axis. Fig. 7 shows the electric resistivity of the oriented $Li_{1.11}Nb_{0.89}Ti_{0.11}O_3$ and $Li_{1.25}Nb_{0.75}Ti_{0.25}O_3$ ceramics. The bar indicates the difference in the measured values for the four specimens. The figure shows that the resistivity parallel to the *c*-axis was higher than that perpendicular to the *c*-axis. The resistivity of $Li_{1.11}Nb_{0.89}Ti_{0.11}O_3$ was higher than that of $Li_{1.25}Nb_{0.75}Ti_{0.25}O_3$. The intergrowth layer is inserted perpendicular to the *c*-axis as shown in Fig. 4 and the number of layers in $Li_{1.25}Nb_{0.75}Ti_{0.25}O_3$ was greater than that in $Li_{1.11}Nb_{0.89}Ti_{0.11}O_3$. From those results, we concluded that the intergrowth layers might form an electric conduction path and that the anisotropic electron conductivity appeared along the *c*-axis.

3.3.2. Microwave dielectric properties

The relationship between Ti content and dielectric properties is plotted in Fig. 8. The dielectric constants are values locating 20–87 which are in good agreement with the 55–78 of M-phase reported [7]. When the value of ε_r was higher in the case of a random specimen, the *Qf* value became lower and it was in good agreement with the normal theory in the random specimen [27]. In the oriented specimen, the *Qf* value was increased with increasing Ti content, with which the measurement direction was parallel to the *c*-axis. On the other hand, the change in the value of ε_r was the same as that of the random specimen. Fig. 9 shows the *Qf* values of LNT

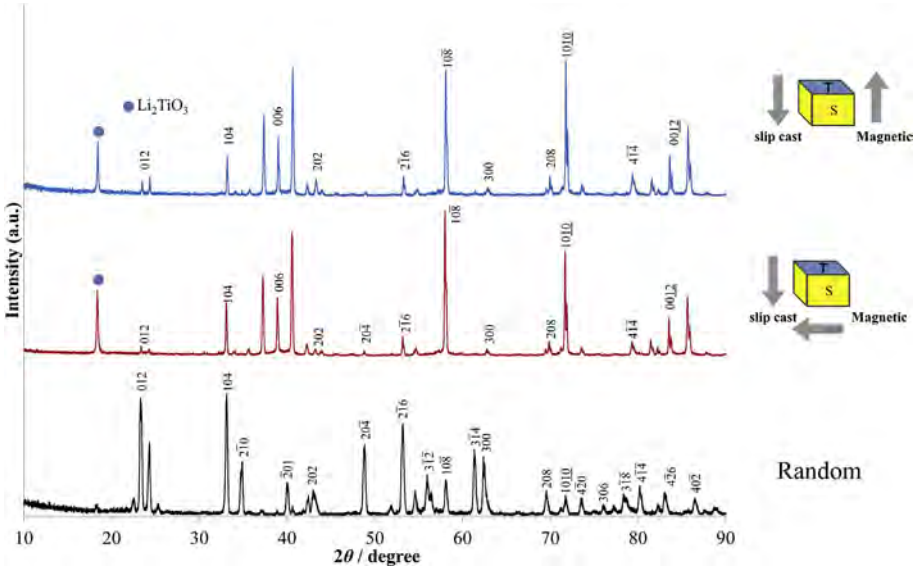

Fig. 6. XRD patterns of $Li_{1.25}Nb_{0.75}Ti_{0.25}O_3$ ceramics on top-plane in magnetic parallel to casting direction and side-plane in the specimen perpendicular to casting direction. The bottom data is a random specimen without a magnetic field.

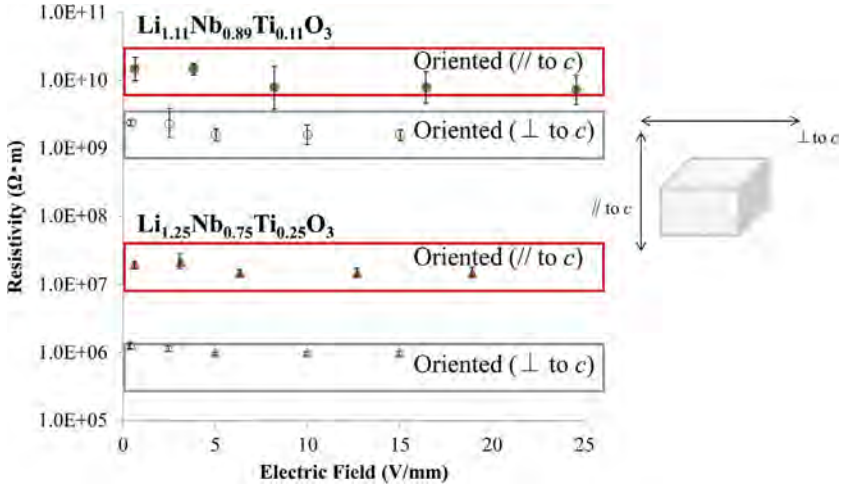

Fig. 7. Electric resistivity of oriented $Li_{1.11}Nb_{0.89}Ti_{0.11}O_3$ and $Li_{1.25}Nb_{0.75}Ti_{0.25}O_3$ ceramics.

Please cite this article in press as: H. Nakano et al., Fabrication and anisotropic electronic property for oriented $Li_{1+x-y}Nb_{1-x-3y}Ti_{x+4y}O_3$ solid solution by slip casting in a high magnetic field, Advanced Powder Technology (2017), http://dx.doi.org/10.1016/j.apt.2017.06.020

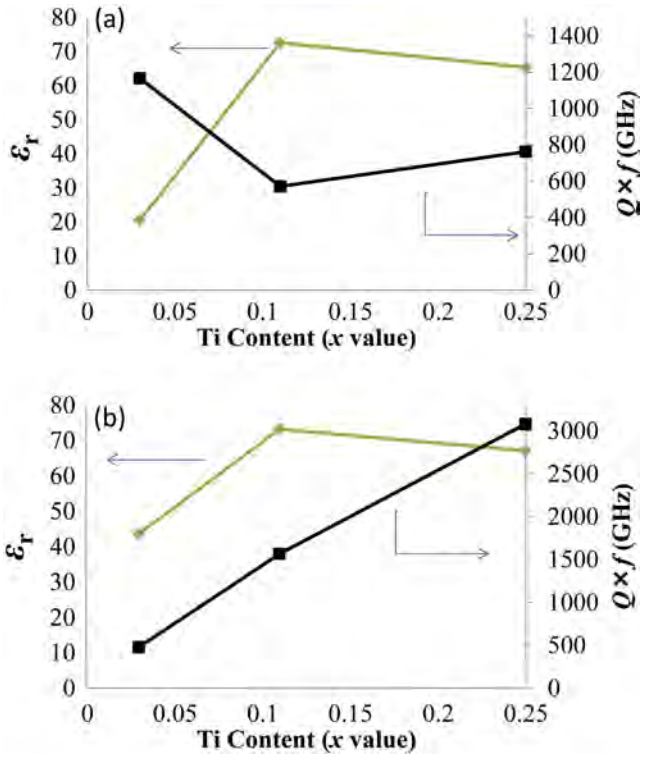

Fig. 8. Relationship between Ti content and dielectric property at microwave frequencies of $Li_{1+x}Nb_{1-x}Ti_xO_3$ random specimen in (a) and oriented specimen in (b).

ceramics parallel to the *c*-axis in (A) and perpendicular to the *c*-axis in (B). R is a random specimen without a magnetic field. The measurement was performed based on the Japanese Industrial Standard [28] using cylindrical samples as pictures in Fig. 9. We found larger values of *Qf* parallel to the *c*-axis in the oriented specimen (A), in which the intergrowth layer of corundum-type $[Ti_2O_3]^{2+}$ was inserted perpendicular to the *c*-axis, in Fig. 9. On the other hand, a large *Qf* value was not found in $Li_{1.03}Nb_{0.97}Ti_{0.03}O_3$ with no superstructure.

4. Discussions

In the present experiment, we successfully fabricated oriented LNT ceramics and found anisotropic electric properties for the first time in the world to the best of our knowledge. The fabrication method of slip casting in a strong magnetic field of 12 T was effective for making the oriented LNT ceramics.

We discuss the reason for the appearance of the anisotropic *Qf* value in the M-phase with a superstructure although ε_r value did not show an anisotropy in the oriented specimen. The *Q* value is closely related to the structure. Some intrinsic factors and extrinsic factors have been reported for improvement of the *Q* value [27]. In order to improve the *Q* value, high ordering, strong bond-strength and small internal-strain are major intrinsic factors which are based on crystal structure. On the other hand, the extrinsic loss factors are defects, impurity, density and electrical conductivity that are based on fabrication conditions. We confirmed that the density, impurity phase and strain were almost the same because of the same processing between A and B in Fig. 9. The electrical conductivity parallel to the *c*-axis was obviously smaller than that perpendicular to the *c*-axis in Fig. 7. The anisotropic property of the electrical conductivity affected the *Qf* value in the same composition. The electric conductivity of $Li_{1.11}Nb_{0.89}Ti_{0.11}O_3$ was lower than that of $Li_{1.25}Nb_{0.75}Ti_{0.25}O_3$. The ratios of Ti^{4+} ion/Ti^{3+} ion in $Li_{1.03}Nb_{0.97}Ti_{0.03}O_3$ and $Li_{1.25}Nb_{0.75}Ti_{0.25}O_3$ were measured by XANES. In general, Ti^{4+} ion changes easily into Ti^{3+} ion by the various Ti-O environments in the material and the change can be analyzed by XANES. The formation of Ti^{3+} ion is related to the electric conductivity. There was Ti^{3+} ion with about 15–20% in the LNT ceramics and the Ti^{3+} ion content increased with the increasing Ti content. The calculated Ti^{3+} ratio may be a higher value than the actual value because the material color is a pure white. This makes the oxygen vacancies in the material with the chemical formula of $Li_{1+x-y}Nb_{1-x-3y}Ti_{x+4y}O_{3-\delta}$. From the XANES data, this ratio of Ti^{4+}/Ti^{3+} was not the important factor for the large *Qf* value. In general, with the increasing the electrical conductivity, the *Qf* value is decreasing. However, the *Qf* value of $Li_{1.25}Nb_{0.75}Ti_{0.25}O_3$ is higher than that of $Li_{1.11}Nb_{0.89}Ti_{0.11}O_3$. Therefore, another factor should contribute to improve the *Qf* value. The internal strain of the crystal structure become larger with increasing the Ti content because of a difference in the crystal structure between the matrix and intergrowth layer, as shown in TEM image (Fig. 4). Consequently, we also could not explain the large *Qf* value by the internal strain.

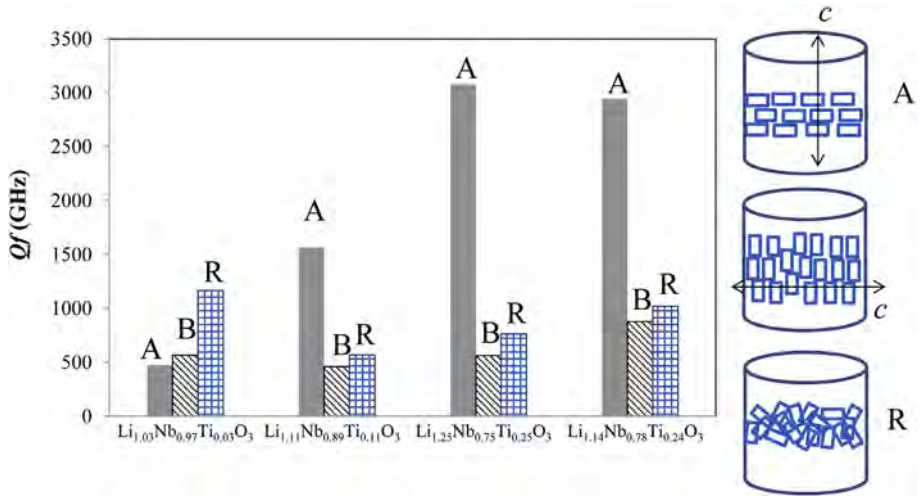

Fig. 9. *Qf* values of LNT ceramics parallel to the *c*-axis in (A), perpendicular to the *c*-axis in (B). R is random specimen.

Please cite this article in press as: H. Nakano et al., Fabrication and anisotropic electronic property for oriented $Li_{1+x-y}Nb_{1-x-3y}Ti_{x+4y}O_3$ solid solution by slip casting in a high magnetic field, Advanced Powder Technology (2017), http://dx.doi.org/10.1016/j.apt.2017.06.020

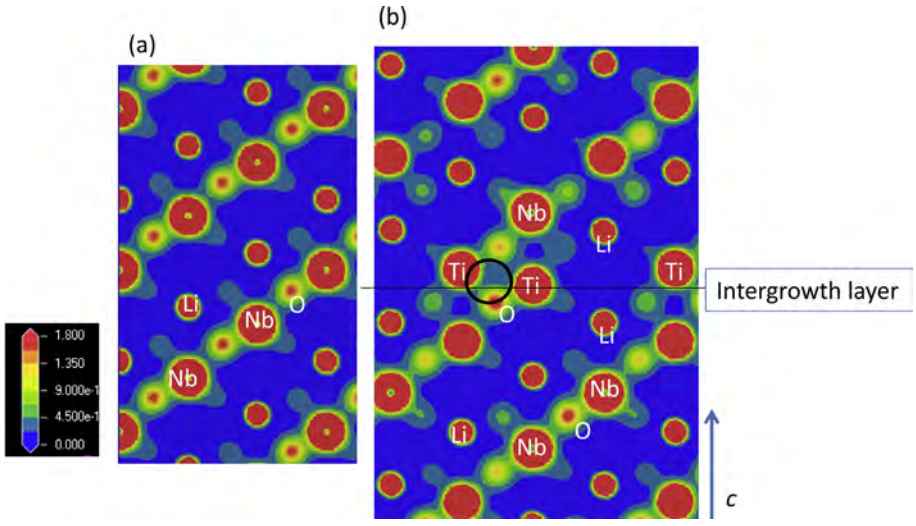

Fig. 10. Electron density map of $LiNbO_3$ in (a) and $Li_{9.5}Nb_{4.4}Ti_{7.1}O_{30}$ in (b) taken from the [100].

Subsequently, the electron densities were calculated using a first-principles calculation, which were carried out using a $LiNbO_3$ and $Li_{9.5}Nb_{4.4}Ti_{7.1}O_{30}$ with 10 layers reported by Farber [6]. The cell sizes were $0.515 \times 0.515 \times 1.386$, and $0.510 \times 1.531 \times 2.319$ nm^3 with a periodic boundary condition in all direction.

Fig. 10 shows electron density maps of $LiNbO_3$ in (a) and $Li_{9.5}Nb_{4.4}Ti_{7.1}O_{30}$ in (b) taken from the [100]. The atomic layer of Nb (Ti)-O-Nb(Ti) layer shifted by insertion of the intergrowth layers. Around the intergrowth layer, higher electron density was observed along the *c*-direction like a covalent bonding as indicated by the circle. Interestingly, the lattice parameter of *c*-axis was significantly decreased with increasing Ti content [25]. In other words, the bonding became stronger along the *c*-axis in the crystal by insertion of the intergrowth layers. In general, with increasing the bonding strength, the relative permittivity (ε_r) decreases and the *Q* value increases [28].

From our results, the high *Qf* value along the *c*-axis was caused by the combination of the anisotropic-electron conductivity and -bonding strength along the *c*-axis in the superstructure with insertion of the intergrowth layers.

5. Conclusion

Oriented balk ceramic was successfully prepared in the Li_2O-Nb_2O_5-TiO_2 system, $Li_{1.03}Nb_{0.97}Ti_{0.03}O_3$, $Li_{1.11}Nb_{0.89}Ti_{0.11}O_3$, $Li_{1.25}Nb_{0.75}Ti_{0.25}O_3$ and $Li_{1.14}Nb_{0.78}Ti_{0.24}O_3$, which has a superstructure except for $Li_{1.03}Nb_{0.97}Ti_{0.03}O_3$. The high degree of orientation was achieved by the good slurries for particle rotation in a high magnetic field. We obtained new findings for anisotropic electron properties from the oriented LNT balk ceramics. The *Qf* value parallel to the *c*-axis was about five times greater than that of perpendicular to the *c*-axis although ε_r value did not show an anisotropy in the oriented specimen. Anisotropic electron conductivity was caused by the intergrowth layers of corundum-type $[Ti_2O_3]^{2+}$, which acted as conduction paths. We concluded from our analytical and simulation results that the large *Qf* value parallel to the *c*-axis was caused from a combination of two factors; one being the anisotropic electron conductivity and the other the anisotropic bonding strength in the superstructure by insertion of the intergrowth layer.

Acknowledgement

This work was partially supported by a Grant-in-Aid for Scientific Research (c) No. 16K06721 (H. N.) by the Japan Society for the Promotion of Science.

References

[1] M.E. Villafuerte-Castrejon, J.A. Gracia, E. Cisneros, R. Valenzuela, A.R. West, New rutile solid solutions $Ti_{1-4x}Li_xM_{3x}O_2$: M = Nb, Ta, Sb, J. Brit. Ceram. Soc. 83 (1984) 143–145.
[2] M.E. Villafuerte-Castrejon, A. Aragon-Pina, R. Valenzuela, A.R. West, Compound and solid-solution formation in the system Li_2O-Nb_2O_5-TiO_2, J. Solid State Ceram. 71 (1987) 103–108.
[3] R.I. Smith, A.R. West, Characterization of an incommensurate LiTiNb oxide, Mater. Res. Bull. 27 (1992) 277–285.
[4] H. Hayashi, H. Nakano, K. Suzumura, K. Urabe, A.R. West, Superstructure in LiTiNb Oxides, Forth Ceram. Soc. 2 (1995) 391–398.
[5] H. Hayashi, K. Urabe, K. Niihara, Preparation of stoichiometric crystalline Li(Nb, Ti)O_3 solid solutions by sol-gel processing with metal alkoxides, Key Eng. Mater. 501 (1999) 161–163.
[6] L. Farber, I. Levin, A. Borisevichi, I.E. Grey, R.S. Roth, P.K. Davies, Structural study of $Li_{1+x-y}Nb_{1-x-3y}Ti_{x+4y}O_3$ solid solutions, J. Solid State Chem. 166 (2002) 81–90.
[7] A.Y. Borisevich, P.K. Davies, Crystalline structure and dielectric properties of $Li_{1+x-y}Nb_{1-x-3y}Ti_{x+4y}O_3$ M-phase solid solutions, J. Am. Ceram. Soc. 85 (2002) 573–578.
[8] Y. Yamamoto, H. Hayashi, T. Sekino, T. Nakayama, T. Kondo, M. Wada, T. Adachi, K. Niihara, Microstructure and dielectric properties of sintered Li-Nb-Ti-O solid solution ceramics having superstructure, Mater. Res. Innov. 7 (2003) 74–79.
[9] H. Hayashi, H. Nakano, Evolution and preparation of $Li_{1+x-y}Nb_{1-x-3y}Ti_{x+4y}O_3$ solid solution with superstructure as new phosphor, J. Alloys Compd. 502 (2010) 360–364.
[10] H. Hayashi, H. Nakano, M.I. Jones, Microstructure and luminescence of Eu-doped $Li_{1+x-y}Nb_{1-x-3y}Ti_{x+4y}O_3$ solid solutions with superstructure, J. Ceram. Soc. Jpn. 118 (3) (2010) 226–230.
[11] H. Nakano, S. Furuya, K. Fukuda, S. Yamada, Synthesis and luminescence enhancement of Eu^{3+}, Sm^{3+} co-doped $Li_{1.11}Ta_{0.89}Ti_{0.11}O_3$ phosphor, Mater. Res. Bull. 60 (2014) 766–770.
[12] Y. Yamamoto, T. Sekino, T. Kusunose, T. Nakayama, Y. Morimoto, S. Miyazawa, K. Niihara, The formation of self-organized regular array microstructure derived from structural anisotropy of phase M solid-solution, J. Cryst. Growth 264 (2004) 445–451.
[13] Y. Yamamoto, T. Sekino, H. Hayashi, T. Nakayama, T. Kusunose, K. Niihara, Synthesis and structure of preferred-orientaed Li_2O-Nb_2O_5-TiO_2 thin film with superstructure, Mater. Lett. 57 (2003) 2702–2706.
[14] Y. Kinemuchi, H. Nakano, H. Kaga, S. Tanaka, K. Uematzu, K. Watari, Microstructural evidence of Hall mobility anisotropy in *c*-axis textured Al-doped ZnO, J. Am. Ceram. Soc. 94 (2011) 2339–2343.
[15] T.S. Suzuki, Y. Sakka, Preparation of oriented bulk 5wt% Y_2O_3-AlN ceramics by slip casting in a high magnetic field and sintering, Scripta Materiallia 52 (2005) 583–586.
[16] T.S. Suzuki, T. Uchikoshi, Y. Sakka, Effect of sintering conditions on microstructure orientation in α-SiC prepared by slip casting in a strong magnetic field, J. Eur. Ceram. Soc. 30 (2010) 2813–2817.
[17] L. Zhang, J. Vleugels, O.V. Biest, Slip casting of alumina suspensions in a strong magnetic field, J. Am. Ceram. Soc. 93 (10) (2010) 3148–3152.
[18] T.S. Suzuki, Y. Sakka, Fabrication of textured titania by slip casting in a high magnetic field followed by heating, Jpn. J. Appl. Phys. 41 (2002) L1272–L1274.
[19] G.W. Brindley, The effect of grain or particle Size on x-ray reflections from mixed powders and alloys, considered in relation to the quantitative determination of crystalline substances by x-ray methods, Philos. Mag. 36 (1945) 347–369.

Please cite this article in press as: H. Nakano et al., Fabrication and anisotropic electronic property for oriented $Li_{1+x-y}Nb_{1-x-3y}Ti_{x+4y}O_3$ solid solution by slip casting in a high magnetic field, Advanced Powder Technology (2017), http://dx.doi.org/10.1016/j.apt.2017.06.020

[20] S.J. Clark, M.D. Segall, C.J. Pickard, P.J. Hasnip, M.J. Probert, K. Refson, M.C. Payne, First-principles methods using CASTEP, Z. Kristallogr. 220 (2005) 567–570.
[21] P. Hohenberg, W. Kohn, Inhomogeneous electron gas, Phys. Rev. 136 (1964) B864–B871.
[22] W. Kohn, L. Sham, Self-consistent equations including exchange and correlation effects, Phys. Rev. 140 (1965) A1133–A1138.
[23] J.P. Perdew, K. Burke, M. Ernzerhof, Generalized gradient approximation made simple, Phys. Rev. Lett. 77 (1996) 3865–3868.
[24] D. Vanderbilt, Soft self-consistent pseudopotentials in a generalized eigenvalue formalism, Phys. Rev. B 41 (1990) 7892–7895.
[25] H. Nakano, T. Saji, M. Yuasa, S. Miyake, M. Mabuchi, Rapid synthesis and structural analysis of Li-Nb-Ti-O solid solutions with superstructure by millimeter-wave heating, J. Ceram. Soc. Jpn. 119 (11) (2011) 808–812.
[26] H. Nakano, K. Watari, Evaluation of grain orientation in textured β-Si_3N_4 ceramics with high thermal conductivity by electron microscopy, Adv. Tech. Mater. Mater. Proc. J. 8 (1) (2006) 67–72.
[27] T. Shimada, Study on dielectric loss of microwave dielectric ceramic, Hitachi kinnzoku gihou 25 (2009) 8–14 (in Japanese).
[28] Japanese Industrial Standard Committee, Testing Method for Dielectric Properties of Fine Ceramics at Microwave Frequency, Japanese Industrial Standard, <https://www.jisc.go.jp/app/JPS/JPSO0020.html> (in Japanese).

Please cite this article in press as: H. Nakano et al., Fabrication and anisotropic electronic property for oriented $Li_{1+x-y}Nb_{1-x-3y}Ti_{x+4y}O_3$ solid solution by slip casting in a high magnetic field, Advanced Powder Technology (2017), http://dx.doi.org/10.1016/j.apt.2017.06.020